Study of optical and dielectric constants of hybrid SnO$_2$ electrospun nanostructures

Wiktor Matysiak[1] · Tomasz Tański[1] · Weronika Smok[1]

Abstract

The aim of this paper was to prepare SnO$_2$ nanowires using electrospinning and calcination processes from a poly(vinylpyrrolidone), dimethylformamide, ethanol and tin(IV) chloride pentahydrate solution. The composite PVP/SnCl$_4$ nanofibers obtained via electrospinning method were dried and calcined in a vacuum to remove the polymer matrix at a temperature of 500 °C for 10 h. Three types of nanowires with a polymer to precursor ratios of 2:1, 1:1, 1:3 were produced. The morphology and chemical composition of as-spun PVP/SnCl$_4$ nanofibers and SnO$_2$ nanowires obtained after heat treatment were carried out using a scanning electron microscope (SEM) with an energy-dispersive spectrometer (EDX). The Fourier-transform infrared spectroscopy (FTIR) spectra of the prepared nanomaterials were also investigated. To determine the topography of PVP/SnCl$_4$ nanofibrous mats, an atomic force microscope (AFM) was used. A 100-fold measurement of the nanowire size showed that, depending on the amount of precursor in the spinning solution, nanowires with diameters ranging from 20 to 260 nm were obtained. The optical property analysis was performed on the basis of absorbance spectra recorded over UV–Vis spectral range. The complex refractive index n and complex dielectric permeability ε of obtained tin oxide nanowires were determined as a function of the radiation energy. Depending on the precursor content in spinning solution, the one-dimensional SnO$_2$ nanostructures were characterised by a refractive index in the range of 1.51–1.56, whereas the dielectric constant ranged from 2.26 to 2.30. The optical properties and the structure of one-dimensional SnO$_2$ nanomaterials allow to use this type of materials in the construction of novel type photovoltaic cells and electronic devices.

Keywords Optical properties · Electrospinning · Nanowires · Nanofibers · Tin oxide

1 Introduction

In recent decades, quasi-one-dimensional (1D) nanostructures, which include nanowires, nanotubes and nanofibers have aroused great interest of scientists due to their diverse application possibilities fibre [1–9]. This is due to the fact that, compared to the micrometre equivalents, many nanostructured materials are characterised by unique mechanical, optical, electrical and magnetic properties. These advantages are the result of their low dimensionality and quantum confinement effect, which is most often observed in semiconductor nanomaterials [10, 11].

Many literature reports suggest that, in addition to popular semiconductor oxides such as ZnO and TiO$_2$, also SnO$_2$ has favourable optical properties [12–14]. Tin oxide nanomaterials are very interesting for the industry due to their large surface-to-volume ratio, n-type semiconductor nature, high optical transmission in the visible range, energy band gap in the range of 3.0–4.0 eV. Thus, SnO$_2$ has a strong transmission in the visible range (0.4 ± 0.8 mm) and a high absorption coefficient in the UV range (104 ± 105 cm^{-1}), the refractive index for thin layers in the range of 1.25–2.3, variable resistivity in a gaseous environment and good mechanical, chemical and thermal stability [15–18].

The various forms of SnO$_2$-based nanostructures are continuously investigated for their optical and electrical properties [19–23]. In 2007, an international research team from Turkey and Israel examined the optical properties of thin SnO$_2$ films produced by the filtered vacuum arc deposition (FVAD) method [24]. During the deposition, the temperature of the substrates was kept at room temperature (RT)

✉ Wiktor Matysiak
    wiktor.matysiak@polsl.pl

1   Department of Engineering Materials and Biomaterials,
    Silesian University of Technology, Konarskiego 18A,
    44-100 Gliwice, Poland

or at 400 °C (hot substrates). The refractive index n of the SnO$_2$ films deposited on RT were 1.87, 1.99 and 1.93 and hot substrates were 1.97, 1.87 and 1.96 for samples prepared at 0.53, 0.67, 0.8 Pa, respectively. Moreover, the extinction coefficients of RT samples in the Vis were 0.01, 0.02, 0.01 and of hot substrates were 0.01 for samples obtained at each pressure.

In 2009, a Pakistani team led by A.F. Khan prepared SnO$_2$ thin films by rf-magnetron sputtering and annealing at various temperatures (100–500 °C) for 15 min [25]. The analysis of optical properties based on the UV–Vis spectrum, show the refractive index ranged from $n_{min} = 1.20$ to $n_{max} = 1.55$ in the UV to near IR regions, the refractive index increased up to 3.00 in the IR region. Moreover, it was observed that the refractive index at $\lambda = 589.3$ nm decreased from 1.50 to 1.35 with annealing temperature increase. The extinction coefficient and the relative permittivity ε were observed to be almost constant with oscillatory behavior up to about 1500 nm, beyond which they rises rapidly in the higher IR region.

Next year, it was observed that the annealing temperature has a significant effect on the structure and optical properties of thin films of SnO$_2$ [26]. To determine the influence of the annealing temperature, SnO$_2$ thin-films were prepared by electron beam evaporation, annealed in 350, 400, 450, 500 and 550 °C for 2 h and subjected to UV–Vis analysis. It has been shown that the refractive index oscillated between 1.25 and 2.30 in the UV, visible and near IR regions. The refractive index measured at $\lambda = 589$ nm was found to increase from 1.35 to 1.88 with increasing annealing temperature showing oscillatory behaviour due to the fringing effect. The authors suggested that, due to the energy band gap and refractive index value ranging from 3.61 to 4.22 eV and 1.25 to 2.30, respectively, SnO$_2$ thin films can be useful as a window material for solar cell applications.

In 2014, Paliwa et al. used the surface plasmon resonance (SPR) technique to examine the optical and electrical properties of SnO$_2$ thin film deposited by the rf-sputtering technique on a gold-coated glass prism [27]. The complex dielectric constant ($\varepsilon_i = \varepsilon_i' + i\varepsilon_i''$) estimated at $\lambda = 633$ nm thin film was about $2.07 + 0.001i$, while the room temperature value of the complex refractive index ($n_i + ik_i$) for SnO$_2$ thin film was $1.439 + 0.032i$. In addition, the authors proved that this type of material can be used for gas sensors, e.g. NH$_3$.

In 2015, Sagadevan and colleagues published the results of their work [28] on the manufacturing of nanocrystalline thin SnO$_2$ films by the chemical bath deposition (CBD) method and they analysed the optical and electrical properties of the films. The refractive index (n), extinction coefficient (K), real dielectric constant (ε_r) and imaginary dielectric constant (ε_i) were determined at $\lambda = 900$ nm and they were equal to 1.56, 0.0032, 2.562 and 0.0025, respectively.

In 2019, a group of scientists from the National Research Center in Egypt deposited oxide films on glass substrates using the low-price spray pyrolysis method, and, among others, SnO$_2$ thin films were prepared and their linear and non-linear optical properties were examined [29]. According to Wemple-DiDomenico (single oscillator model) model, the values of the zero-frequency dielectric constant (ε_s) and the static refractive index (n_s) were calculated as equal to 3.50 and 1.72, respectively.

The above considerations indicate that the multifunctionality and the ability to control the optical properties of SnO$_2$ nanostructures made them useful as electrodes in lithium-ion (LIB) batteries, gas sensors, photocatalysts for purifying water from dyes and ions, as well as elements of novel photovoltaic solar cells [30–35].

According to our best knowledge, there were no contributions to the detailed analysis of the optical properties of electrospun SnO$_2$ nanowires. Thus, a small number of publications and premises for a large specific surface area and unique optical properties of one-dimensional SnO$_2$ nanostructures prompted the authors to produce them using the electrospinning method with subsequent thermal treatment. Atomic force microscopy (AFM), Fourier-transform infrared spectroscopy (FTIR), scanning electron microscopy (SEM) and X-ray energy dispersion spectroscopy (EDX) are used to characterise the morphology, structure and chemical composition of the obtained nanomaterials. In addition, optical properties are analysed based on the UV–Vis spectrum of the obtained SnO$_2$ nanowires. The recorded absorbance spectra allow to determine the refractive index n, the real part of the refractive index n and the imaginary part k of the refractive index as a function of wavelength, dielectric permittivity ε and the real and imaginary part ε_r and ε_i of the dielectric constant. The obtained values are consistent with those published so far [28].

2 Materials and methodology

To prepare the spinning solutions, the following reagents purchased from Sigma-Aldrich were used: poly(vinylpyrrolidone) (PVP, purity of 99%, Mw = 1,300,000 g·mol^{-1}), ethanol (EtOH, purity 99.8%), N, N-dimethylformamide (DMF, purity of 99.8%) and tin (IV) chloride pentahydrate (SnCl$_4$·5H$_2$O, purity 98%).

At first, three poly(vinylpyrrolidone) solutions were prepared by adding PVP to ethanol in an amount corresponding to 8% wt. relative to the total weight of solvents and stirring for 48 h. At the same time, different amounts of tin oxide precursor were dissolved in DMF and after 48 h of stirring added to the PVP solution and mixed for another 24 h to obtain homogeneous solutions. The final solution contains EtOH:DMF in a mass ratio of 1:1 and PVP:SnCl$_4$·5H$_2$O in mass ratio of 2:1, 1:1, 1:3 (type 1, 2, 3, respectively).

The nanofibrous composite PVP/SnCl$_4$ mats were manufactured using FLOW—Nanotechnology Solutions Electrospinner

2.2.0–500 device, maintaining constant parameters: voltage and distance between electrodes of 22 kV and 15 cm and a flow rate of 0.4 ml·h^{-1}. To remove the organic matrix, the as-obtained composite nanomats were calcinated in a high-temperature vacuum furnace HT-2100-G-Vac-Graphit-Special, at 500 °C for 10 h with a heating rate of 10 °C·min^{-1} for all samples; after that the samples were left in the furnace to cool (Fig. 1).

To evaluate the morphology and chemical composition of the manufactured materials, a Zeiss Supra 35 scanning electron microscope (SEM) with a EDAX Trident XM4 series x-ray spectrometer (EDX) were used. Based on the SEM images, the diameters of the randomly selected composite and nanowires were measured using a Digital Micrograph. The structure analysis was investigated using FTIR Nicolet 6700/8700 spectrophotometer. Moreover, to observe the surface morphology of obtained one-dimensional nanostructures, an atomic force microscope (AFM) park system was used.

The absorbance measurements were carried out using a UV–Vis Evolution 220 spectrophotometer by Thermo-Scientific Company. The optical properties were analysed on the basis of UV–Vis absorbance spectra, and values of refractive index n, real n′ and imaginary k part of the refractive index, complex dielectric permittivity ε, and real and imaginary part ε_r and ε_i of the dielectric permittivity were determined for the 1D SnO$_2$ nanomaterials.

3 Results and discussion

3.1 Morphology, topography and chemical composition analysis

In Fig. 2, the SEM images of the PVP/SnCl$_4$ nanofibres with the corresponding fibre diameter histograms are shown. Based on the SEM images, it was observed that all obtained samples were characterised by a constant diameter along the entire length of the smooth fibre. However, the sample observation for the lowest precursor concentration revealed that, unlike the other two, many fibres were found that stuck together, and a small number of defects in the form of beads was detected. The appearance of these defects is due to the hydrolysis and condensation reactions during mixing of the polymer and precursor solutions. A too low viscosity of the prepared spinning solution was also indicated. In the case of samples obtained from 1 and 2 solution types, it can be stated that the appropriate parameters of the solution and the electrospinning process were selected. In addition, analysing the diameter sizes based on a 100-fold measurement of randomly selected composite nanofibers, it can be seen that, as the precursor concentration increases, the average diameter (d_{avg}) of the nanofiber increases from 55 nm for the sample with the lowest precursor concentration to 121 nm for the sample with the highest concentration. The nanomaterial from the type 3 solution consisted of fibres with the largest variation in diameter values, which ranged from 40 to 260 nm, and the most numerous group—40% were fibres with diameters from 140 to 180 nm. In the case of samples obtained from type 1 and 2 solutions, most (42 and 37%) fibres had a diameter in the range of 20–80 nm and 50–120 nm, respectively.

The topography analysis of the as-obtained composite PVP/SnCl$_4$ nanofibres was carried out using an atomic force microscope. In Fig. 2, it is shown that all the nanofibrous mats display a web-like structure consisting of many randomly entangled and well-individualised fibres with the micro- and nanosized dimension. The results obtained using AFM allow to draw the same conclusions as in the case of SEM analysis that all of PVP/SnCl$_4$ nanofibers had a cylindrical shape and a smooth surface with no visible defects, agglomeration of precursor particles or impurities. Unlike SEM images for the sample with the least amount of
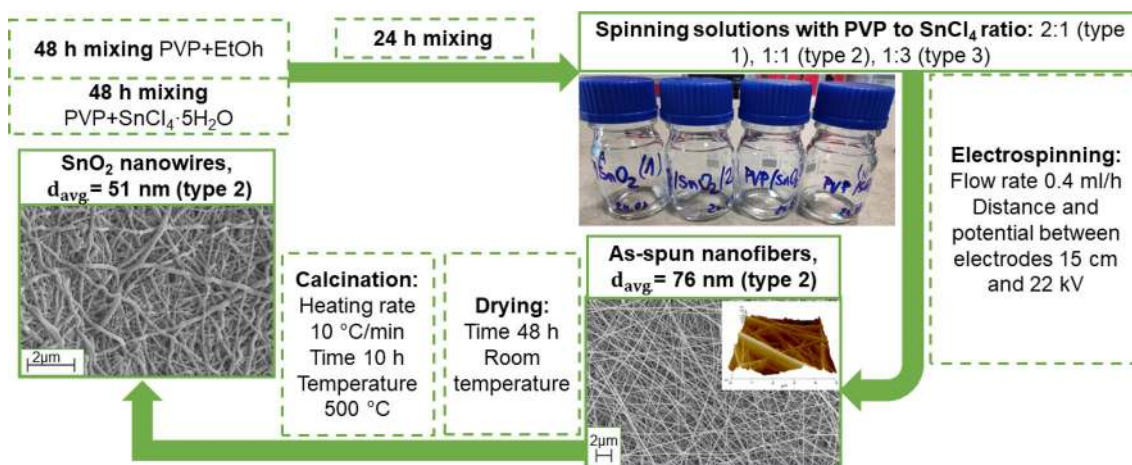

Fig. 1 Methodology of SnO$_2$ nanowires fabrication via electrospinning and sol–gel methods
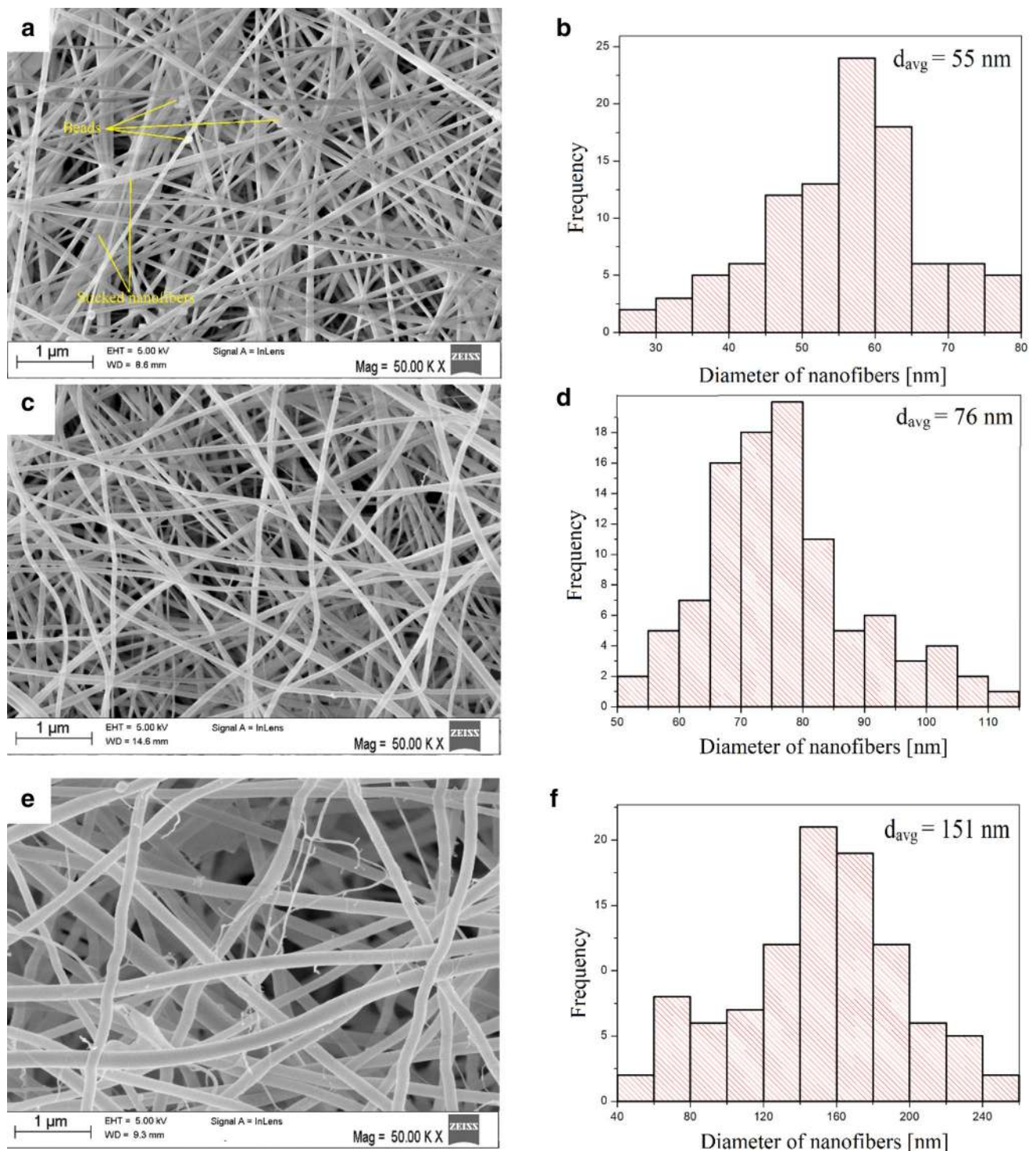
Fig. 2 SEM images of PVP/SnCl$_4$ nanofibres obtained after electrospinning from solution type: **a** one; **c** two; **d** three and corresponding to them histograms of diameter distribution (**b**, **d**, **f**)

precursor, there are no visible defects in the form of beads. This is because defects are not visible in every area of the sample. In addition, the relationship between the diameter increases with the increase in precursor concentration in the spinning solution is also observable. The values for the apparent diameter of the nanofibres measured with AFM were higher than those obtained by SEM, and this is probably due to a bump effect of nearby fibres. The SEM and

AFM analysis confirmed that homogeneous composite PVP/SnCl$_4$ nanomats were produced by electrospinning method (Fig. 3).

The EDX spectrum recorded for nanofibers before calcination with PVP:SnCl$_4$ ratio 1:1 is shown in Fig. 4a. The noticeable Sn peak comes from the presence of precursor particles, just like the peak of Cl which precursor contains much more. In the spectrum made for corresponding SnO$_2$ nanowires after calcination at 500 °C, there is no Cl peak derived from the precursor, while a characteristic peak of oxygen appeared (Fig. 4b), which confirms the formation of pure SnO$_2$ nanowires. The analysis of the structure of SnO$_2$ nanostructures before and after calcing with FTIR is shown in Fig. 5. The spectrum recorded for the sample before calcination process shows peaks characteristic of PVP polymer presence O–H, C–N, C=O and C–H bonds, which are visible at 1290, 1460, 1640 and 2931 cm^{-1}, respectively. Furthermore, a wide band typical for Sn–O binding was observed at 612 cm^{-1}, which is due to the presence of the precursor. Analysing the FTIR spectrum of the nanostructures after the calcining process, it can be seen that only one major peak from Sn–O binding occurs at position 668 cm^{-1}, which like EDX results confirms the SnO$_2$ nanowires preparation.
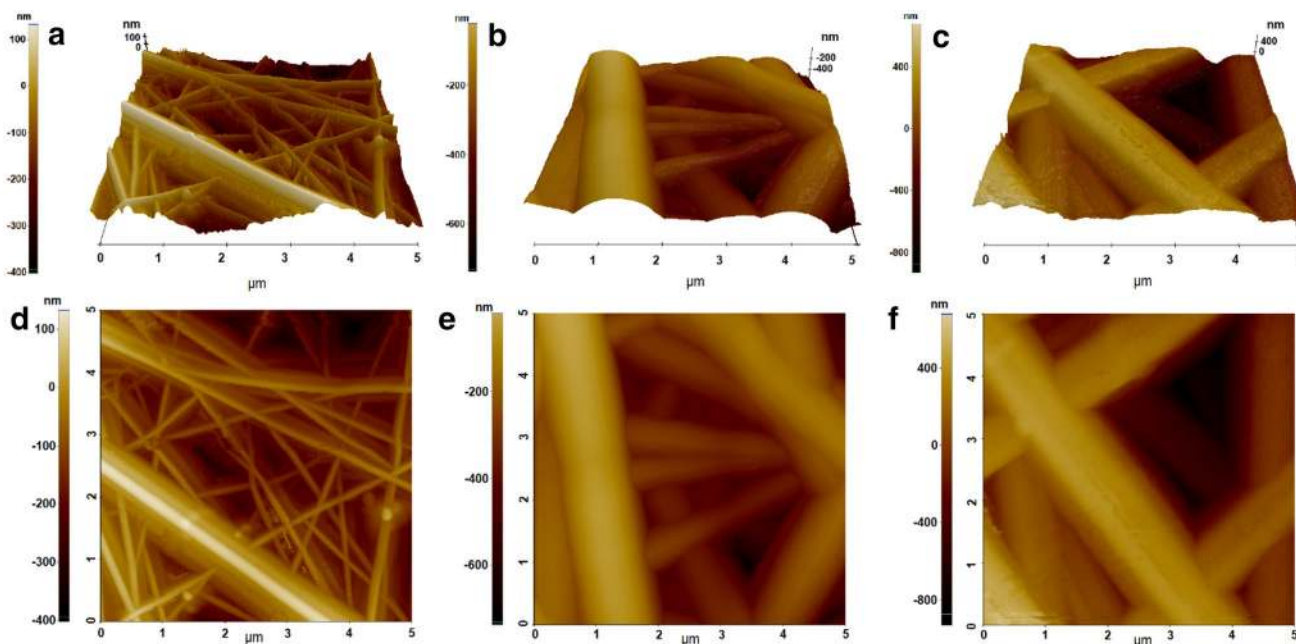

Fig. 3 AFM surface characterisation of PVP/SnCl$_4$ nanofibres type: **a**, **d** one; **b**, **e** two; **c**, **f** three before calcination
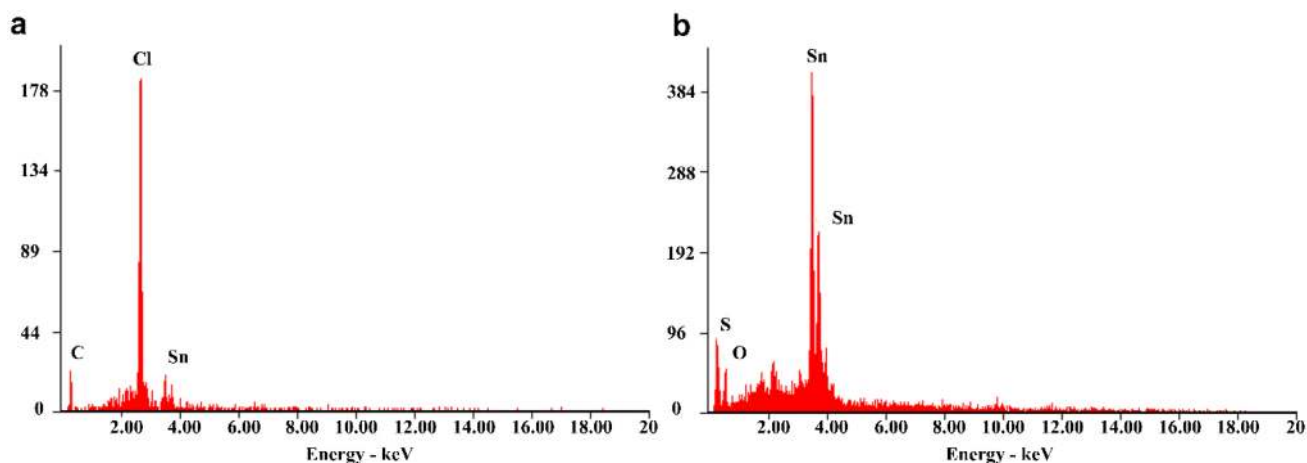

Fig. 4 EDX spectra of obtained: **a** type 2 nanofibres before calcination, **b** type 2 nanowires after calcination
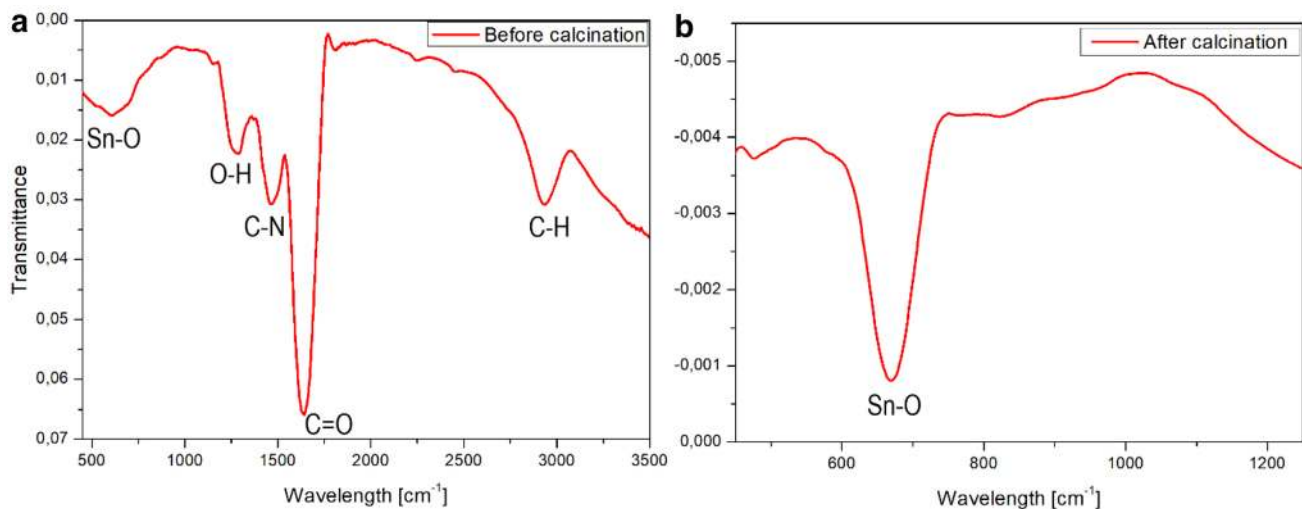
Fig. 5 FTIR spectra of obtained: **a** type 2 nanofibres before calcination, **b** type 2 nanowires after calcination

The SEM images of SnO_2 nanowires, produced by calcination of $PVP/SnCl_4$ nanofibers at 500 °C, and the histogram based on a 100-fold measurement of diameters of randomly selected wires is shown in Fig. 6. The morphology analysis of SnO_2 nanowires showed that, compared to the fibres before calcination, they were characterised by a rough surface with numerous crystalline protuberances increasing the specific surface. In addition, the observation of nanowires obtained after calcination of type 1 nanofibres showed significant size of SnO_2 agglomerates formed from beads present before calcination. Based on a 100-fold diameter meas-

3.2 Optical studies

Based on the received spectra of absorbance as a function of the wavelength using the method presented in [36, 37], the following optical and electrical properties were determined: the refractive index n, real n' and imaginary k part of the refractive index as a function of the wavelength, complex dielectric permeability ε, and real and imaginary part ε_r and ε_i of the dielectric permeability as a function of the radiation wavelength of the produced SnO_2 one-dimensional nanostructures, using the final equations in the following form:

$$n = \left\{ 2n_p \frac{10^{-A(\lambda)_{max}} - 10^{-A(\lambda)_{min}}}{10^{-A(\lambda)_{max}} 10^{-A(\lambda)_{min}}} + \frac{n_p^2 + 1}{2} + \left[\left(2n_p \frac{10^{-A(\lambda)_{max}} - 10^{-A(\lambda)_{min}}}{10^{-A(\lambda)_{max}} 10^{-A(\lambda)_{min}}} + \frac{n_p^2 + 1}{2} \right)^2 - n_p^2 \right]^{1/2} \right\}^{1/2}, \tag{1}$$

urement, it was noticed that the average diameter of mid (51 nm) and the highest precursor concentration (101 nm) nanowires are smaller than those of corresponding nanofibres, which is the result of organic phase degradation. In the case of type 1 nanowires, an increase of more than twofold from 55 to 120 nm in diameter is observed, which is caused by sintering of previously stuck fibres.

where n_p—the refractive index of the substrate used, λ — wavelength, A—absorbance,

$$n'(\lambda) = \left\{ \frac{4R(\lambda)}{[R(\lambda) - 1]^2} - \left[\frac{1}{4\pi} \lambda \ln \frac{1}{T(\lambda)} \right]^2 \right\}^{1/2} - \frac{R(\lambda) + 1}{R(\lambda) - 1}, \tag{2}$$

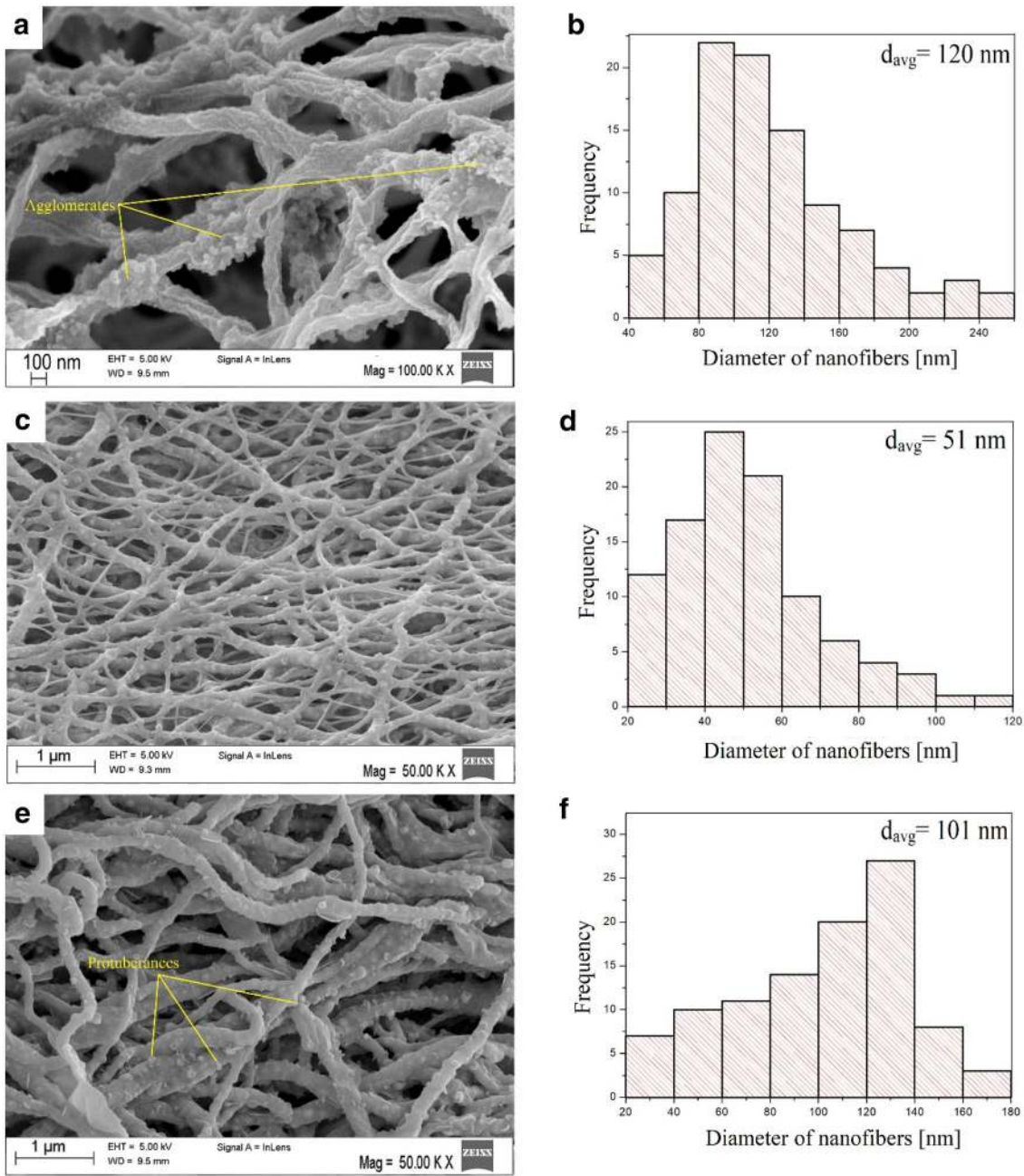where R—reflectance, T—transmittance,

Fig. 6 SEM images SnO₂ nanowires obtained after calcination in 500 °C type: **a** one, **c** two, **d** three nanofibres and corresponding to them histograms of diameter distribution (**b**, **d**, **f**)

$$k(\lambda) = \frac{1}{4\pi} \lambda \ln \frac{1}{10^{-A(\lambda)}}, \tag{3}$$

$$\varepsilon = 2n_p \frac{10^{-A(\lambda)}{}_{max} - 10^{-A(\lambda)}{}_{min}}{10^{-A(\lambda)}{}_{max} 10^{-A(\lambda)}{}_{min}} + \frac{n_p{}^2 + 1}{2} + \left[\left(2n_p \frac{10^{-A(\lambda)}{}_{max} - 10^{-A(\lambda)}{}_{min}}{10^{-A(\lambda)}{}_{max} 10^{-A(\lambda)}{}_{min}} + \frac{n_p{}^2 + 1}{2} \right) - n_p{}^2 \right]^{1/2}, \tag{4}$$
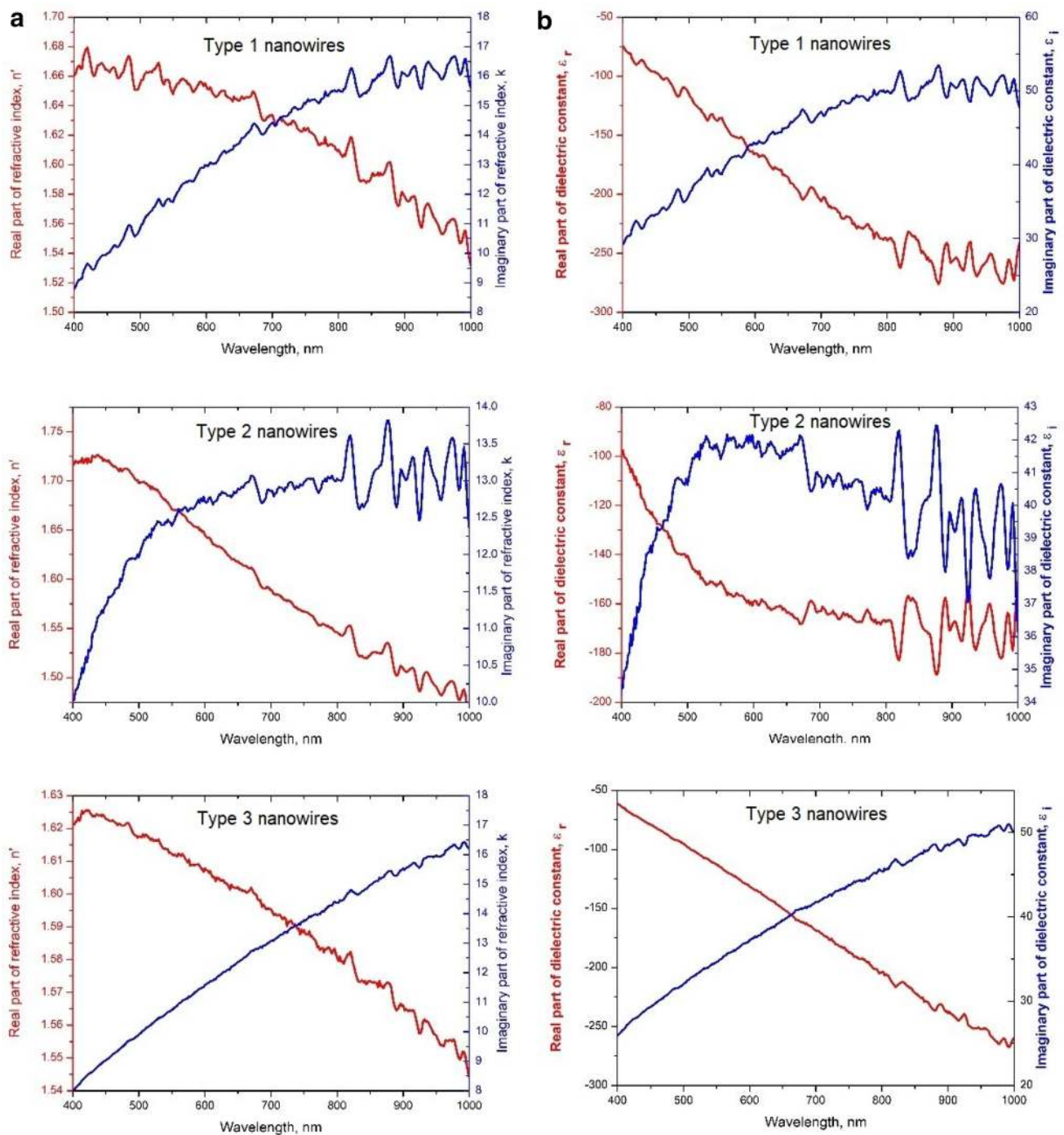
Fig. 7 The dependences of the real $n'(\lambda)$ and imaginary $k(\lambda)$ parts (**a**) of the refractive index determined and of the real $\varepsilon_r(\lambda)$ and imaginary $\varepsilon_i(\lambda)$ parts (**b**) of the dielectric constant for the one-dimensional tin oxide nanomaterials

$$\varepsilon_r(\lambda) = \left\{ \left\{ \frac{4R(\lambda)}{[R(\lambda)-1]^2} - \left[\frac{1}{4\pi}\lambda\ln\frac{1}{T(\lambda)}\right]^2 \right\}^{1/2} - \frac{R(\lambda)+1}{R(\lambda)-1} \right\}^2 - \left[\frac{1}{4\pi}\lambda\ln\frac{1}{T(\lambda)}\right]^2, \tag{5}$$

Table 1 Refractive index and dielectric permittivity obtained for the electrospun 1D SnO₂ nanomaterials

Parameter	SnO₂ nanowires		
	Type of spinning solutions		
	Type 1	Type 2	Type 3
n	1.51	1.52	1.50
ε	2.28	2.30	2.26

As-spun nanomats were dried and calcined in a vacuum furnace at 500 °C for 10 h, which resulted in the formation of SnO₂ nanowires. The analysis of SEM and AFM morphology show that smooth, homogeneous nanofibres with diameters ranging from 30 to 240 nm were obtained. The composite nanofibres produced from the solution with the smallest amount of precursor were characterised by the smallest average diameter. The SnO₂ nanowires obtained as a result of calcining were characterised by a developed, rough surface with numerous crystalline protuberances.

$$\varepsilon_i(\lambda) = 2\left\{ \left\{ \frac{4R(\lambda)}{[R(\lambda)-1]^2} - \left[\frac{1}{4\pi}\lambda\ln\frac{1}{T(\lambda)} \right]^2 \right\}^{1/2} - \frac{R(\lambda)+1}{R(\lambda)-1} \right\} \left[\frac{1}{4\pi}\lambda\ln\frac{1}{T(\lambda)} \right]. \tag{6}$$

Based on the above equations and UV–Vis spectra, recorded for the semiconductor one-dimensional SnO₂ nanostructures the spectral dependences of the $n'(\lambda)$, $k(\lambda)$ and $\varepsilon_r(\lambda)$, $\varepsilon_i(\lambda)$, were determined (Fig. 7). The values of the refractive index (Eq. 1), dielectric permittivity (Eq. 4) for the electrospun one-dimensional tin oxide nanostructures, and the obtained results are presented in Table 1.

The refractive indexes analysis performed for all three groups of electrospun one-dimensional SnO₂ nanostructures showed that the calculated values are similar fibre (Table 1). In addition, using the recorded UV–Vis spectra and Eq. (4), the dielectric constants of the produced SnO₂ nanowires were determined, which were, respectively, 2.30, 2.28 and 2.26 for nanostructures obtained from 2, 1 and 3 of the spinning solution type (Table 1). The calculated values of refractive indices and dielectric constants for electrospun one-dimensional SnO₂ nanostructures coincide with the values obtained on the basis of absorbance spectra by Suresh Sagadevan and Jiban Podder ($n = 1.56$, $\varepsilon = 2.562$) [28] in the case of two-dimensional tin oxide nanostructures. Slight difference in the optical constant values of the one-dimensional SnO₂ nanostructures in the form of an electrospun thin films (this study) and solid thin layer obtained by the chemical bath deposition (CBD) method [28], probably resulted from the morphology of the nanomaterials. The obtained results proved the possible future application of this type of 1D tin oxide nanostructures in the production of photovoltaic cells or optoelectronic devices.

4 Conclusion

This study demonstrates the fabrication of SnO₂ one-dimensional nanostructures by a combination of two simple methods: sol–gel and electrospinning. The morphology and optical properties were analysed. In the first stage, a PVP/DMF/EtOH/SnCl₄ solutions were prepared, which were electrospun to obtain the composite PVP/SnCl₄ nanofibrous mats.

The comparison of the diameters of the obtained nanowires showed that the smallest average diameter was characteristic of the wires obtained as a result of electrospinning a solution with a 1:1 precursor to polymer ratio.

As a result of the UV–Vis spectra analysis of SnO₂ nanowires, it was shown that, regardless of the concentration of the precursor in the solution from which they were obtained, they have similar values of refractive index (1.50–1.52) and dielectric constant (2.26–2.30). These values are similar to those presented so far in the literature, which confirms that the method used allows obtaining good quality 1D SnO₂.

The hybrid method combining electrospinning with the sol–gel technique has many advantages over other methods of manufacturing one-dimensional nanomaterials, because it enables relatively simple, reproducible and above all cheap production of ready-to-use nanomaterials, which without the need for functionalisation or purification are characterised by comparable or better physical properties than their equivalents obtained by other methods.

The above considerations indicate that low-cost SnO₂ nanowires due to their beneficial optical properties can be used as photoanodes of modern dye cells, electronic components or photocatalysts.

References

1. Z.R. Dai, Z.W. Pan, Z.L. Wang, Ultra-long single crystalline nanoribbons of tin oxide. Solid State Commun. **118**(7), 351–354 (2001)
2. H.W. Kim, S.H. Shim, Branched structures of tin oxide one-dimensional nanomaterials. Vacuum **82**(12), 1395–1399 (2008)
3. L. Wang, G. Yang, S. Peng, J. Wang, W. Yan, S. Ramakrishna, One-dimensional nanomaterials toward electrochemical sodium-ion storage applications via electrospinning. Energy Storage Mater. (2019). https://doi.org/10.1016/j.ensm.2019.09.036
4. L. Yu, S. Ruan, X. Xu, R. Zou, J. Hu, One-dimensional nanomaterial-assembled macroscopic membranes for water treatment. Nano Today **17**, 79–95 (2017)
5. T. Tański, P. Jarka, M. Szindler, A. Drygała, W. Matysiak, M. Libera, Study of dye sensitized solar cells photoelectrodes consisting of nanostructures. Appl. Surf. Sci. **491**, 807–813 (2019)
6. L. Mai, J. Sheng, L. Xu, S. Tan, J. Meng, One-dimensional hetero-nanostructures for rechargeable batteries. Acc. Chem. Res. **51**(4), 950–959 (2018)
7. T. Shimizu, Self-assembly of discrete organic nanotubes. Bull. Chem. Soc. Jpn. **91**(4), 623–668 (2018)
8. K.V. Dorozhkin, G.E. Dunaevsky, S.Y. Sarkisov, V.I. Suslyaev, O.P. Tolbanov, V.A. Zhuravlev et al., Terahertz dielectric properties of multiwalled carbon nanotube/polyethylene composites. Mater. Res. Express **4**(10), 106201 (2017)
9. P.M. Sylenko, A.M. Shlapak, S.S. Petrovska, O.Y. Khyzhun, Y.M. Solonin, V.V. Atuchin, Direct nitridation synthesis and characterisation of Si_3N_4 nanofibers. Res. Chem. Intermed. **41**(12), 10037–10048 (2015)
10. W. Matysiak, T. Tański, Novel bimodal ZnO (amorphous)/ZnO NPs (crystalline) electrospun 1D nanostructure and their optical characteristic. Appl. Surf. Sci. **474**, 232–242 (2019)
11. N.S. Mohammad, Understanding quantum confinement in nanowires: basics, applications and possible laws. J. Phys Condens. Matter **26**(42), 423202 (2014)
12. W. Matysiak, T. Tański, M. Zaborowska, Manufacturing process, characterisation and optical investigation of amorphous 1D zinc oxide nanostructures. Appl. Surf. Sci. **442**, 382–389 (2018)
13. T. Wang, Y. Gao, T. Tang, H. Bian, Z. Zhang, J. Xu et al., Preparation of ordered TiO_2 nanofibres/nanotubes by magnetic field assisted electrospinning and the study of their photocatalytic properties. Ceram. Int. **45**(11), 14404–14410 (2019)
14. V.R. Bandi, C.M. Raghavan, B. Kumar Grandhe, S.S. Kim, K. Jang, D.S. Shin et al., Synthesis, structural and optical properties of pure and rare-earth ion doped TiO_2 nanowire arrays by a facile hydrothermal technique. Thin Solid Films **547**, 207–211 (2013)
15. S. Das, S. Kar, S. Chaudhuri, Optical properties of SnO_2 nanoparticles and nanorods synthesized by solvothermal process. J. Appl. Phys. **99**(11), 114303 (2006)
16. V.S. Jahnavi, S.K. Tripathy, A.R. Rao, Structural, optical, magnetic and dielectric studies of SnO_2 nano particles in real time applications. Phys. B **565**, 61–72 (2019)
17. X. Zhang, Y. Rui, Y. Wang, J. Xu, H. Wang, Q. Zhang, P. Müller-Buschbaum, SnO_2 nanorod arrays with tailored area density as efficient electron transport layers for perovskite solar cells. J. Power Sources **402**, 460–467 (2018)
18. S. Hamzaoui, M. Adnane, Effects of temperature and rf power sputtering on electrical and optical properties of SnO_2. Appl. Energy **65**(1–4), 19–28 (2000)
19. N. Ahmad, S. Khan, M.M.N. Ansari, Optical, dielectric and magnetic properties of Mn doped SnO_2 diluted magnetic semiconductors. Ceram. Int. **44**(13), 15972–15980 (2018)
20. A. Ahmed, M.N. Siddique, T. Ali, P. Tripathi, Influence of reduced graphene oxide on structural, optical, thermal and dielectric properties of SnO_2 nanoparticles. Adv. Powder Technol. **29**(12), 3415–3426 (2018)
21. M.A. Yıldırım, S.T. Yıldırım, E.F. Sakar, A. Ateş, Synthesis, characterisation and dielectric properties of SnO_2 thin films. Spectrochim. Acta Part A Mol. Biomol. Spectrosc. **133**, 60–65 (2014)
22. D. Varshney, K. Verma, Effect of stirring time on size and dielectric properties of SnO_2 nanoparticles prepared by co-precipitation method. J. Mol. Struct. **1034**, 216–222 (2013)
23. N. Mazumder, A. Bharati, S. Saha, D. Sen, K.K. Chattopadhyay, Effect of Mg doping on the electrical properties of SnO_2 nanoparticles. Curr. Appl. Phys. **12**(3), 975–982 (2012)
24. E. Çetinörgü, S. Goldsmith, R.L. Boxman, The effect of substrate temperature on filtered vacuum arc deposited zinc oxide and tin oxide thin films. J. Cryst. Growth **299**(2), 259–267 (2007)
25. A.F. Khan, M. Mehmood, A.M. Rana, M.T. Bhatti, A. Mahmood, Optical characterisation of rf-magnetron sputtered nanostructured SnO_2 thin films. Chin. Phys. Lett. **26**(7), 077803 (2009)
26. A.F. Khan, M. Mehmood, M. Aslam, M. Ashraf, Characteristics of electron beam evaporated nanocrystalline SnO_2 thin films annealed in air. Appl. Surf. Sci. **256**(7), 2252–2258 (2010)
27. A. Paliwal, A. Sharma, M. Tomar, V. Gupta, Dielectric properties of SnO_2 thin film using SPR technique for gas sensing applications. In: Conference Papers in Science, vol. 2014 (Hindawi 2014)
28. S. Sagadevan, J. Podder, Optical and electrical properties of nanocrystalline SnO_2 thin films synthesized by chemical bath deposition method. Soft Nanosci. Lett. **5**, 55–64 (2015)
29. I.M. El Radaf, T.A. Hameed, T.M. Dahy, Synthesis, structural, linear and nonlinear optical properties of chromium doped SnO_2 thin films. Ceram. Int. **45**(3), 3072–3080 (2019)
30. Z.H. Bakr, Q. Wali, J. Ismail, N.K. Elumalai, A. Uddin, R. Jose, Synergistic combination of electronic and electrical properties of SnO_2 and TiO_2 in a single SnO_2–TiO_2 composite nanofibre for dye-sensitized solar cells. Electrochim. Acta **263**, 524–532 (2018)
31. S.R. Ch, L. Zhang, T. Kang, Y. Lin, Y. Qiu, Annealing impact on the structural and optical properties of electrospun SnO_2 nanofibres for TCOs. Ceram. Int. **44**(5), 4586–4591 (2018)
32. D. Lei, M. Zhang, Q. Hao, L. Chen, Q. Li, E. Zhang, T. Wang, Morphology effect on the performances of SnO_2 nanorod arrays as anodes for Li-ion batteries. Mater. Lett. **65**(8), 1154–1156 (2011)
33. X. Kuang, T. Liu, D. Shi, W. Wang, M. Yang, S. Hussain et al., Hydrothermal synthesis of hierarchical SnO_2 nanostructures made of superfine nanorods for smart gas sensor. Appl. Surf. Sci. **364**, 371–377 (2016)
34. K. Ahn, D. Pham-Cong, H.S. Choi, S.Y. Jeong, J.H. Cho, J. Kim et al., Bandgap-designed TiO_2/SnO_2 hollow hierarchical nanofibres: synthesis, properties, and their photocatalytic mechanism. Curr. Appl. Phys. **16**(3), 251–260 (2016)
35. I.M. Mohamed, V.D. Dao, A.S. Yasin, H.S. Choi, N.A. Barakat, Synthesis of novel SnO_2@ TiO_2 nanofibres as an efficient photoanode of dye-sensitized solar cells. Int. J. Hydrog. Energy **41**(25), 10578–10589 (2016)
36. W. Matysiak, T. Tański, Analysis of the morphology, structure and optical properties of 1D SiO_2 nanostructures obtained with sol–gel and electrospinning methods. Appl. Surf. Sci. **489**, 34–43 (2019)
37. T. Tański, W. Matysiak, Synthesis of the novel type of bimodal ceramic nanowires from polymer and composite fibrous mats. Nanomaterials **8**(3), 179 (2018)